Invited Paper

Silicon photonic Bragg-grating couplers for optical communications

Wei Shi[a*], Venkat Veerasubramanian[b], David V. Plant[b], Nicolas A. F. Jaeger[c], and Lukas Chrostowski[c]

[a]Department of Electrical and Computer Engineering and the Center for Optics, Photonics, and Lasers (COPL), Université Laval, Québec, Canada
[b]Department of Electrical and Computer Engineering, McGill University, Montreal, Canada
[c]Department of Electrical and Computer Engineering, The University of British Columbia, Vancouver, Canada

ABSTRACT

We discuss recent progress and challenges in realizing Bragg-grating devices on the submicron silicon-on-insulator platform for next-generation optical communications applications, such as on-chip optical interconnects and signal processing. In particular, we focus on grating-assisted, wavelength-selective couplers, known as contra-directional couplers (contra-DCs). In contrast to conventional two-port Bragg gratings operating in the reflection mode, contra-DCs are four-port devices with very weak backreflections and, therefore, can be easily integrated with other photonic components on a chip. In order to provide a reliable on-chip wavelength-division multiplexing (WDM) solution for high-speed optical interconnects, we have developed high-performance add-drop filters and, furthermore, wavelength multiplexers/demultiplexers with combined advantages of flat-top responses, low insertion loss (< 1 dB), and low crosstalk (< -23 dB). These WDM devices are ultra-compact and highly tolerant to temperature fluctuations (up to ± 50 ^{0}C), showing great potential for large-scale integration and low-power consumption. We further discuss a novel four-port Bragg photonic resonator for high-speed, low-power optical switching. Using a coupler-chirped design with uniform Bragg gratings, we have recently achieved an on-chip, continuously tunable photonic delay line with low insertion loss. These system-orientated devices indicate great potential for large-scale integration of Bragg-grating-defined functions using CMOS-compatible silicon photonics technology.

Keywords: Add-drop filters, Bragg gratings, contra directional couplers, delay line, optical communications, silicon photonics, wavelength-division multiplexing

1. INTRODUCTION

Bragg gratings are widely used in optical communication systems for applications such as wavelength-division multiplexing (WDM),[1] dispersion compensation,[2] narrow-linewidth lasers,[3] gain equalization,[4] and optical signal processing.[5] As silicon photonics has quickly emerged as a main-stream technology for integrated photonic circuits, there is great interest to develop integrated Bragg gratings on the silicon-on-insulator (SOI) platform.[6–9] Silicon photonic Bragg gratings can be implemented by physically corrugating silicon waveguides. A series of Bragg grating devices have been developed on the submicron SOI platform using CMOS-compatible fabrication process. Dense-WDM (DWDM) filters were demonstrated with bandwidths as narrow as 0.4 nm.[8] High-Q resonators were obtained using phase-shifted Bragg gratings showing Q factors of 10^5 and higher.[10,11] In order to achieve long Bragg filters on a silicon chip, spiral grating structures were developed to minimize their footprints.[12] Sampled Bragg gratings were also demonstrated for tunable lasers and comb filters.[13,14]

While significant progress has been made in integrated Bragg gratings, many challenges remain. One of the major issues associated with their applications in large-scale photonic systems is that they operate in reflection mode, which requires optical circulators for add-drop operation. Integrated circulators/isolators have yet to be developed on a silicon chip. Off-chip optical circulators may dramatically increase the cost and complexity of

*E-mail: wei.shi@gel.ulaval.ca

Next-Generation Optical Networks for Data Centers and Short-Reach Links, edited by Atul K. Srivastava, Proc. of SPIE Vol. 9010, 90100F · © 2014 SPIE
CCC code: 0277-786X/14/$18 · doi: 10.1117/12.2044096

integrated photonic systems. Grating-assisted asymmetric waveguide couplers have no, or very weak, reflection at the operating wavelength, therefore, they intrinsically function as wavelength-selective add-drop filters (four-port devices), circumventing the need for optical isolators or circulators.[15] Particularly, asymmetric couplers with contra-directional coupling, namely, contra-directional couplers (contra-DCs), are appealing due to their compactness in comparison with their co-directional counterparts. Contra-DCs in planar optical waveguides were first investigated based on silica and III-V materials[15–19] and have recently been implemented on the SOI platform.[20–22] As high coupler asymmetry is important for filter performance (e.g., out-of-band rejection ratio, free spectral range),[23] submicron SOI provides a flexible platform to implement contra-DCs. This is because SOI waveguides with a typical height of 200 to 300 nm are very sensitive to dimensional variations, therefore, one can obtain large effective-index differences between two SOI waveguides by simply varying their widths. Integrated silicon photonic contra-DCs have enabled many novel applications such as on-chip optical-pulse compression,[24] single-longitudinal-mode microring resonators,[25] single-band, flat-top add-drop filters,[26] and four-port photonic resonators.[27] These devices can be easily cascaded and integrated with other photonic components for large-scale integrated photonic circuits.

In this paper, we review our recent work on silicon photonic contra-DCs and their applications in optical communications. In Section 2, we review the principle of add-drop filters using contra-DCs and their design and optimization on the SOI platform. To address crucial issues in submicron Bragg gratings, we show novel designs, such as out-of-phase gratings and coupler-apodization for significantly improved performance. In Section 3, we present a few contra-DC enabled on-chip devices, such as ultra-compact, high-performance coarse WDM demultiplexers, four-port Bragg resonators and electrically tunable filters, and integrated tunable delay lines, and discuss their applications for optical interconnects and integrated microwave photonic systems. Unless specified, all the devices demonstrated in this paper are based on 220 nm SOI wafers.

2. PRINCIPLE AND OPTIMIZATION

2.1 Principle

The schematic of a contra-DC is shown in Fig. 1. It consists of two waveguides with different widths to suppress the broadband, co-directional coupling between the transverse modes of the coupler, $\mathbf{E}_1(x, y)$ and $\mathbf{E}_2(x, y)$. With the assistance of Bragg gratings within the asymmetric coupler, efficient contra-directional coupling takes place at the wavelength that satisfies the phase-match condition (i.e., drop-port central wavelength, λ_D):

$$\lambda_D = \Lambda(n_1 + n_2) \tag{1}$$

where n_1 and n_2 are the effective indices of the first and second modes of the asymmetric coupler; Λ is the grating pitch. There exist another two Bragg wavelengths due to the backreflections of individual modes, λ_a and λ_b, which limit the spectral range that can be used for a WDM link. In Section 2.3, we will show an anti-reflection design to suppress these backreflections.

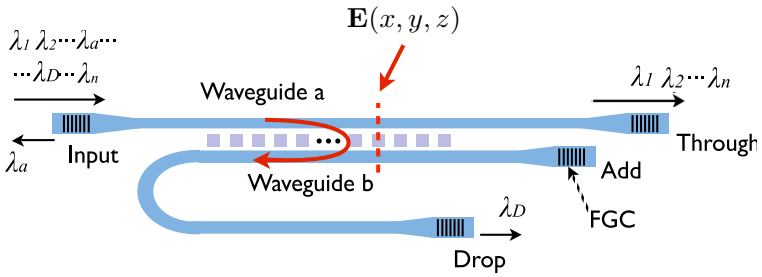

Figure 1. Schematic drawing of a contra-DC-based add-drop filter. The field, $\mathbf{E}(x, y, z)$, in the coupler region, can be decomposed into the transverse modes, $\mathbf{E_1}$ and $\mathbf{E_2}$, as shown by Eq. 2.

A comprehensive coupled-mode model[28] for contra-DCs includes forward propagating (+) and backward propagating (-) waves for the two modes. The electric field in the contra-DC is given by

$$\mathbf{E}(x, y, z) = [A^+(z)e^{-i\hat{\beta}_1 z} + A^-(z)e^{j\hat{\beta}_1 z}]\mathbf{E}_1(x, y) + [B^+(z)e^{-j\hat{\beta}_2 z} + B^-(z)e^{j\hat{\beta}_2 z}]\mathbf{E}_2(x, y) \tag{2}$$

where $\hat{\beta} = \beta - i\alpha$ represents the complex propagation constant; β and α are the real propagation constant and the propagation loss, respectively; A^+, B^+, A^-, and B^- are the field amplitudes as functions of the longitudinal position, z.

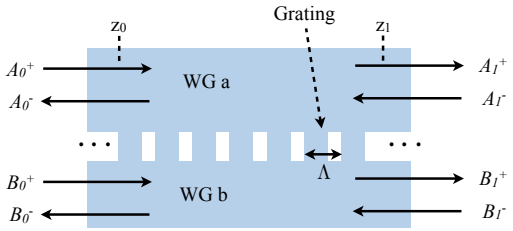

Figure 2. Schematic drawing of a contra-directional coupler. A uniform grating is formed between two different-sized waveguides. The arrows indicate the optical waves in the coupled-mode analysis.

The coupled-mode equations are

$$\frac{dA^+}{dz} = -j\kappa_{11}A^- e^{j2\triangle\hat{\beta}_1 z} - j\kappa_{12}B^- e^{j(\triangle\hat{\beta}_1+\triangle\hat{\beta}_2)z} \tag{3a}$$

$$\frac{dB^+}{dz} = -j\kappa_{12}A^- e^{j(\triangle\hat{\beta}_1+\triangle\hat{\beta}_2)z} - j\kappa_{22}B^- e^{j2\triangle\hat{\beta}_2 z} \tag{3b}$$

$$\frac{dA^-}{dz} = j\kappa_{11}^* A^+ e^{-j2\triangle\hat{\beta}_1 z} + j\kappa_{12}^* B^- e^{-j(\triangle\hat{\beta}_1+\triangle\hat{\beta}_2)z} \tag{3c}$$

$$\frac{dB^-}{dz} = j\kappa_{12}^* A^+ e^{-j(\triangle\hat{\beta}_1+\triangle\hat{\beta}_2)z} + j\kappa_{22}^* B^- e^{-j2\triangle\hat{\beta}_2 z} \tag{3d}$$

where κ_{11} and κ_{22} are the coefficients for the backreflections of $\mathbf{E}_1$ and $\mathbf{E}_2$, respectively; κ_{12} ($\kappa_{21} = \kappa_{12}^*$) is the coefficient for the contra-directional coupling between $\mathbf{E}_1$ and $\mathbf{E}_2$. These coupling coefficients are given by

$$\kappa_{11} = \frac{\omega}{4}\iint \mathbf{E}_1^*(x,\ y)\cdot\triangle\varepsilon_1(x,\ y)\ \mathbf{E}_1(x,\ y)\ dx\ dy \tag{4a}$$

$$\kappa_{12} = \kappa_{21}^* = \frac{\omega}{4}\iint \mathbf{E}_1^*(x,\ y)\cdot\triangle\varepsilon_1(x,\ y)\ \mathbf{E}_2(x,\ y)\ dx\ dy \tag{4b}$$

$$\kappa_{22} = \frac{\omega}{4}\iint \mathbf{E}_2^*(x,\ y)\cdot\triangle\varepsilon_1(x,\ y)\ \mathbf{E}_2(x,\ y)\ dx\ dy \tag{4c}$$

The above equations can be solved using the transfer-matrix method for contra-DCs with various apodization and chirp profiles.[28,29]

2.2 Add-drop Filters on Silicon

Contra-DCs can be implemented in sidewall-modulated strip waveguides and slab-modulated rib waveguides. Their cross-sectional structures are illustrated in Fig. 3. Strip-waveguides need only one etch and can have a large spacing between the Bragg wavelengths because of their strong dispersions. However, due to the strong optical confinement, sidewall modulated gratings require small corrugations (tens of nanometers) that are sensitive to fabrication errors. Slab-modulated rib waveguides have lower effective-index contrast allowing for larger corrugations (hundreds of nanometers). Therefore, they are more suitable for narrow-bandwith filters that require more precise control of weak coupling coefficients.[21] For example, Fig. 4 shows the SEM image and measured spectra of a contra-DC in slab-modulated rib waveguides fabricated at imec, Belgium, using 193-nm lithography.[21] The insertion loss is mainly due to the fiber-grating couplers (FGCs) used in the experiment. A narrow bandwidth of 0.6 nm was obtained with an insertion loss of less than 1dB. The bandwidth of a contra-DC can be controlled by varying the grating magnitudes or the coupler gap. A wide range of bandwidths, from sub-nanometers to greater than 10 nm, were obtained experimentally.[21,22,30] The spectral responses of these add-drop filters can be engineered using well established Bragg-grating techniques, such as apodization and chirping. This indicates that they can be used as flexible building blocks for integrated photonic systems.

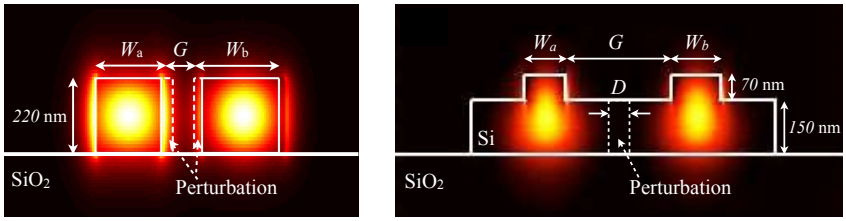

(a) (b)

Figure 3. Cross-sectional structures of contra-DCs in (a) sidewall-modulated strip waveguides and (b) slab-modulated rib waveguides, with the coupled modes calculated using a mode solver.

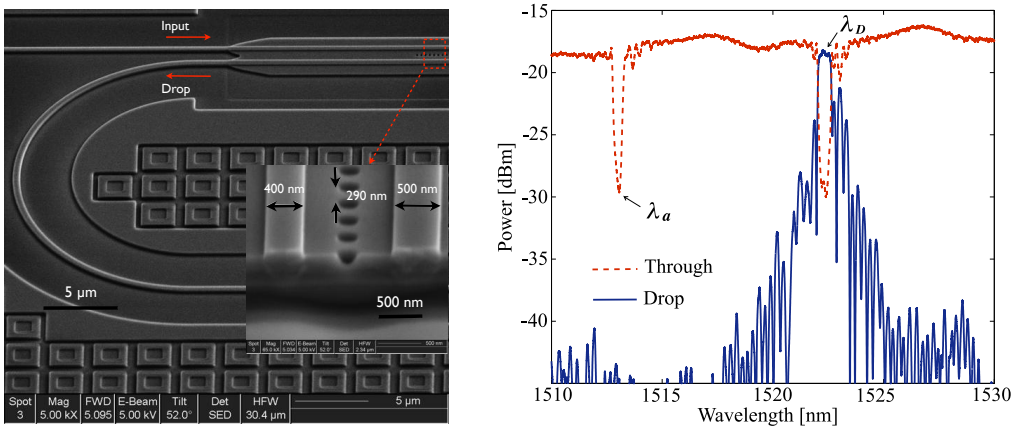

Figure 4. A contra-DC in slab-modulated rib waveguides: (a) SEM image; (b) measured spectra (input power of 1 mW with an insertion loss of ∼17 dB, mostly due to the FGCs). The device has a rib height of 70 nm and the following parameters: $W_a = 400$ nm, $W_b = 500$ nm, $\Lambda = 290$ nm, $N = 4000$, $D = 220$ nm, and $G = 1$ μm.

2.3 Anti-Reflection Design for Single-Band Operation

As shown in Fig. 4, while there is a single passband in the drop-port response, the through-port spectrum shows two notches that correspond to the contra-directional coupling (λ_D) and backreflections (λ_a). Add-drop operation of the contra-DC relies on the detuning of λ_a from λ_D. Nevertheless, the spacing between the two wavelengths limits the spectral range available for applications such as WDM networks. To address this issue, we proposed to use out-of-phase gratings to suppress the backreflections.[26,30] Figure 5 (b) shows an example of an anti-reflection (AR) contra-DC fabricated using e-beam lithography. Gratings are formed on both the internal and external sidewalls of the coupler. As revealed by Eq. 4, the coupling coefficients depend on the overlap between the optical fields and the dielectric perturbation. While the contra-directional coupling coefficient (κ_{12}) is determined by the internal gratings, the backreflections depend on both the internal and external gratings. In order to suppress the backreflections, the gratings on the external sides of the coupler are detuned from the internal gratings by half the pitch to obtain destructive interference of the reflected waves. To verify the performance of this AR design, a conventional contra-DC, where only the internal sidewalls are corrugated, was fabricated on the same wafer. The measured results are shown in Fig. 5. We can see that, for the conventional contra-DC, the spectral spacing between λ_D and λ_a is about 20 nm. In contrast, the AR contra-DC shows only one notch across a wide span of 200 nm, indicating strong suppression of the backreflections. This unique single-band, add-drop operation is attractive for integrated WDM systems because it allows for the uninterrupted increase of WDM channels.

2.4 Coupler-Apodized Bragg Add-Drop Filters

Apodization is a well known technique to suppress grating sidelobes. However, it is challenging to accurately control the grating profile in high-index-contrast silicon waveguides, where dielectric perturbations (10 to 100 nm) are comparable to or smaller than the lithography wavelength (e.g., 193 or 248 nm). The impact of the lithography smoothing effects[31] and fabrication-induced phase errors[32] on silicon photonic Bragg gratings has been throughly

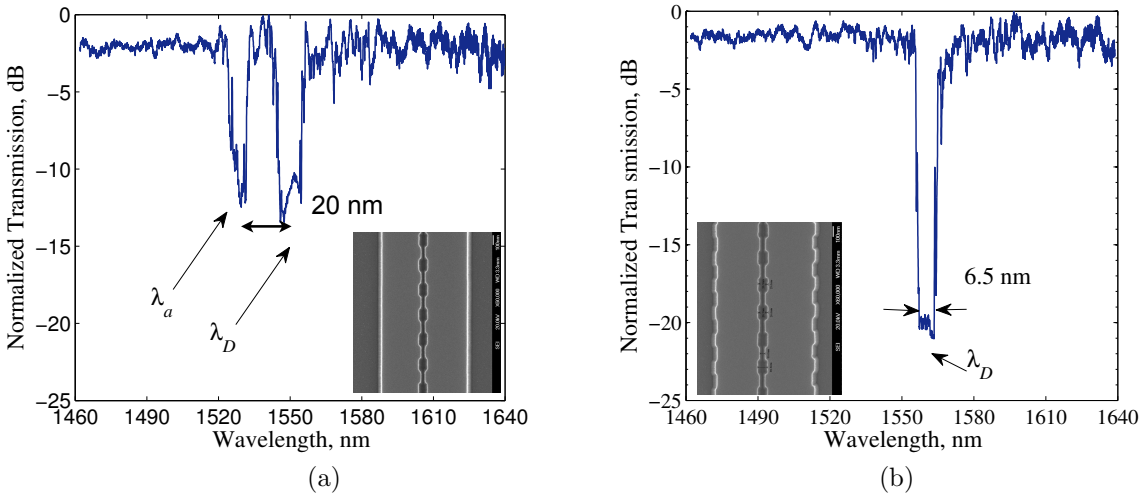

Figure 5. (a) Measured through-port spectrum of a conventional contra-DC with gratings between the two waveguides; (b) Measured through-port spectrum of an anti-reflection contra-DC with out-of-phase gratings to suppress backreflections. Insets: SEM images.

investigated. To overcome this issue, we recently proposed using a tapered coupler gap to implement apodization in contra-DCs.[29] Because the feature size of the coupler gap (in the range of 100 nm to 1 μm) is usually larger than the waveguide perturbations, this coupler apodization method enables a higher tolerance to fabrication errors. By keeping the perturbation amplitude constant, the lithography effects are constant throughout the apodization profile, leading to higher reliability. A coupler anodized contra-DC is shown in Fig. 6(a). The coupler gap, G, is designed as a Gaussian function of the position, z, in the longitudinal direction:

$$G(z) = G_{min} + 2H[1 - e^{\frac{-a(z-0.5L)^2}{L^2}}] \tag{5}$$

where G_{min} is the minimum gap (at the waist of the coupler) and is chosen to be 1 μm in this design. The constant H is chosen to be 2 μm. The index, a, determines the curvatures of the two waveguides and, thus, the apodization strength. An apodized coupler with $a = 2.5$ was fabricated and measured. The fabrication was performed by imec, Belgium (accessed via ePIXfab), using 193-nm lithography. The measured drop-port spectrum is illustrated in Fig. 6(b), showing strong side-lobe suppression, with the highest side-lobe of being about -30 dB (at about 5-nm detuning from the central wavelength). This result is a significant improvement to the previously demonstrated apodized Bragg grating filters on submicron SOI wafers (10 to 15 dB).[9]

3. APPLICATIONS

3.1 Wavelength-Division (De-)Multiplexers for On-Chip Optical Interconnects

The challenge of WDM on silicon lies in the sensitivity of silicon photonic waveguides to fabrication errors and temperature fluctuations. For example, the central wavelength of a microring resonator may vary by a few nanometers across a few millimetre distance on the same die due to fabrication non-uniformity. In addition, optical filters on silicon have a temperature dependence of approximately 0.1 nm/^{o}C,[33] which is significant for applications (e.g., integrated optical interconnects) where a large temperature swing ($\pm$ 30 to 50 ^{0}C) is expected. As a result, significant power could be consumed on thermal trimming and dynamic tuning of WDM filters. Therefore, while DWDM has higher spectral efficiency, CWDM is preferred for short-reach applications, such as data centres and high-performance computers. This is because CWDM has wider channel bandwidths and spacings (e.g., ITU-T G.694.2 standardizes a 20-nm channel-spacing grid), which is tolerant to wavelength drifts and requires no strict thermal control or cooling. Most demonstrated integrated silicon CWDM demultiplexers are on micron-scale silicon waveguides,[34,35] which are relatively bulky (on a scale of 10 mm^2). On submicron silicon wafers, CWDM demultiplexers were recently demonstrated using planar concave gratings[36] and curved

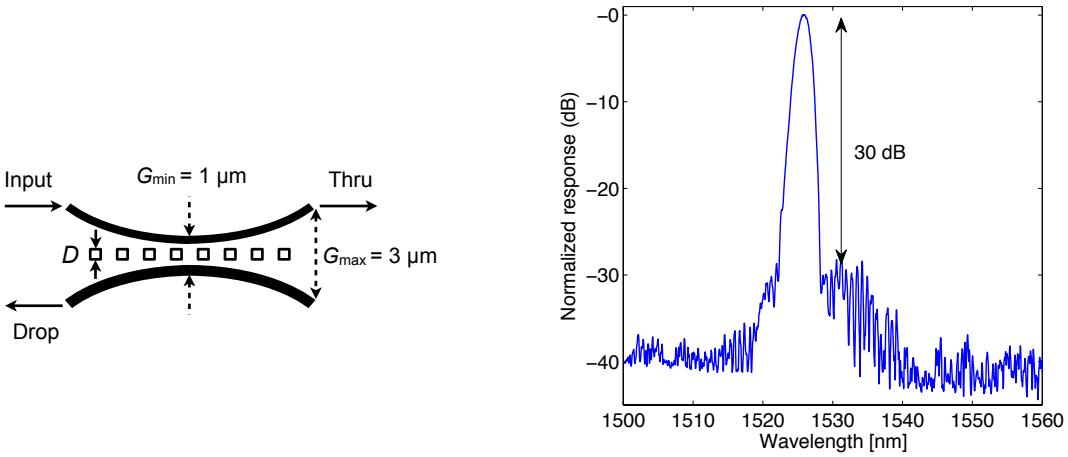

(a) (b)

Figure 6. (a)Schematic of the coupler-apodized contra-DC with uniform Bragg gratings; (b) Measured drop-port response of the coupler-apodized contra-DC.

sidewall gratings.[37] However, these devices suffer from non-flat-top responses, which makes athermal operation challenging.

Using cascaded contra-DCs, we designed 4-channel CWDM demultiplexers. A schematic is shown in Fig. 7. Since the contra-DCs perform as reciprocal add-drop filters, the same design can also perform multiplexing. Each contra-DC consists of sidewall-modulated strip waveguides with an average coupler gap of 100 nm. The input waveguide and drop waveguides are 440 nm and 560 nm wide, respectively. Out-of-phase gratings are used to suppress backreflections, as discussed in Section 2.3. Each coupler has 1,000 grating periods (N) that are apodized with a Gaussian profile such that D for the nth period is given by

$$D = D_{max} e^{-a\frac{(n-0.5N)^2}{N^2}} \tag{6}$$

where a D_{max} of 12 and 24 nm is used for the input and output waveguides, respectively, and a is a variable index. Uniform grating pitches of 312, 320, 328, and 336 nm are chosen for the first to fourth channels, respectively, aiming at a 20-nm wavelength grid spacing. Devices with $a = 5$ and $a = 10$ were fabricated using e-beam lithography. As shown in Fig. 8, the measured spectra have flat-top responses with insertions losses of less than 1 dB for all of the channels. For $a = 5$, the 1 dB bandwidths are greater than 10 nm, allowing for a large temperature swing of over $\pm$ 50 ^{0}C. The adjacent channel crosstalk is improved from -15 dB to -23 dB when the apodization index is increased from 5 to 10, with the tradeoff of smaller bandwidths (8 nm). Performance improvement is anticipated through optimizing the apodization/chirp function.

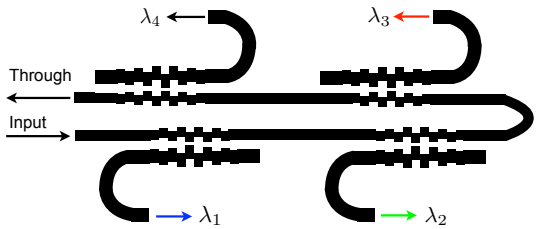

Figure 7. Schematic of the CWDM demultiplexer using apodized contra-DCs.

3.2 Four-Port Tunable Bragg Resonators

Phase-shifted Bragg gratings are widely used in optical communications and signal processing.[38] High-Q resonators in phase-shifted (PS) Bragg gratings with measured Q factor of up to 1×10^5 were demonstrated.[10]

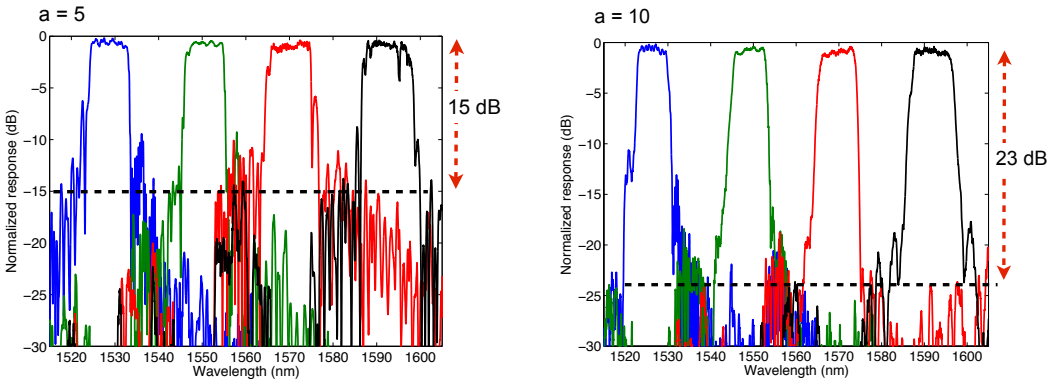

(a) (b)

Figure 8. (a)Measured spectral responses of a CWDM demultiplexer with apodization $a = 5$; (b) $a = 10$.

Photonic resonators with add-drop operation are desired for integrated applications to avoid use of on-chip isolators. We proposed an add-drop resonator using PS contra-DCs and verified its functionality through a thorough coupled-mode analysis.[28] Its principle of operation is illustrated Fig. 9. The structure can be seen as an uniform contra-DC with a π phase shift in the middle of the grating, or a half-wavelength high-index layer sandwiched between two contra-DCs. This phase shift results in a ring-like cavity with distributed optical feedback provided by the contra-DCs. As compared to conventional phase-shifted Bragg gratings (two-port devices), where the optical resonance happens inside a single waveguide, this contra-DC photonic resonator has a circular feedback loop between two waveguides, enabling a narrowband add-drop filter (four-port device).

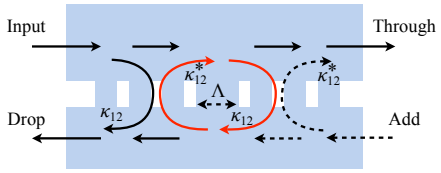

Figure 9. Schematic drawing of a PS contra-DC. The red arrows indicate the resonant loop of the optical cavity.

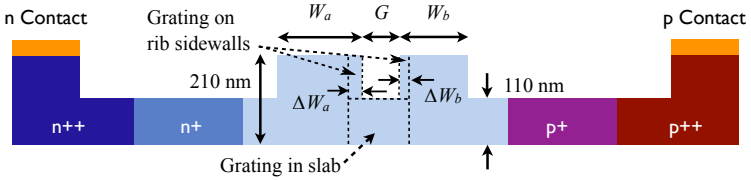

Figure 10. Cross-section of the PS contra-DC with a p-i-n configuration.

We designed a PS contra-DC that was fabricated at BAE Systems using 248-nm lithography. As shown in Fig. 3.2, both the sidewalls and slab between the two rib waveguides are modulated for strong coupling. The two waveguides are 600 nm (W_a) and 400 nm (W_b) in width with corrugation amplitudes on the rib sidewalls of 50 nm and 30 nm, respectively. The device is 210 μm in length with 700 grating periods. A p-i-n structure is used for high-speed tuning or switching through carrier injection. The measured spectra are shown in Fig. 11(a). The through-port response shows a resonance peak at the center of the stopband, i.e., the drop-port central wavelength λ_D. The resonant notch in the drop-port response has an extinction ratio of over 24 dB. As shown in Fig. 11(b), the resonance peak can be dynamically tuned by varying the current. A tuning efficiency of -0.73 nm/mA was measured. As the current is increased from 0 to 1.5 mA, the Q factor is reduced from 7,000 to 2,000 due to higher free-carrier absorption. A small-signal modulation measurement gave a 3-dB bandwidth of 90 MHz. The frequency response can be significantly improved if the depletion mode is used, as this low Q design allows for a photon-lifetime-determined cutoff frequency of ~25 GHz.

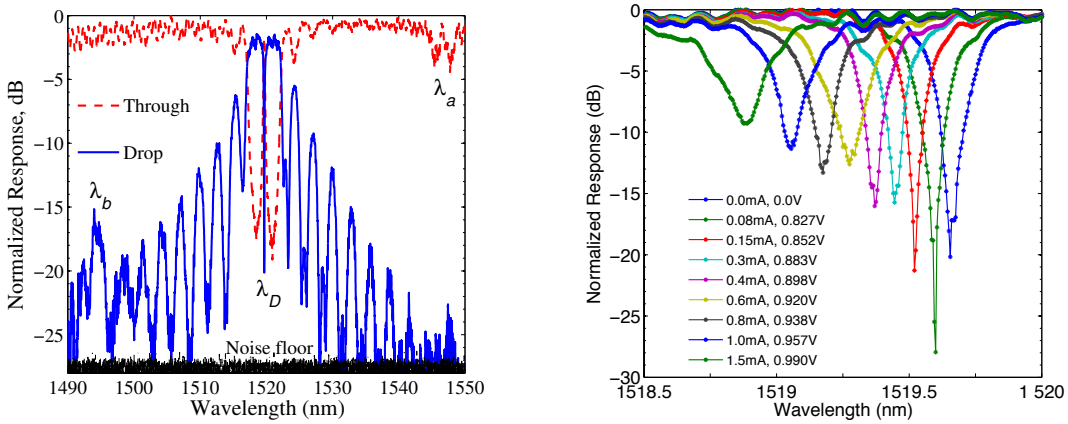

(a) (b)

Figure 11. (a) Measured spectra of a PS contra-DC; (b) Measured drop-port spectra for various currents.

3.3 Integrated Tunable Optical Delay Lines

Tunable optical delay lines are critical components for dispersion compensation[2] and optical signal processing.[39] While they are conventionally implemented using chirped fiber Bragg gratings,[2] there has been significant interest in realizing integrated tunable delay lines, especially on the SOI platform, for on-chip optical interconnects.[40,41] Various solutions based on microring resonators and photonic crystals have been investigated, showing large delays and high tunability.[41,42] However, they suffer from high losses, typically 35 to 100 dB/ns,[40–42] which is a major obstacle to their adoption in systems. Chirped waveguide Bragg gratings have low losses (< 10 dB/ns)[43] and, thus, are attractive for photonic integrated circuits. A continuously tunable delay line using linearly chirped Bragg gratings was recently demonstrated in micrometer-scale SOI waveguides.[44] Realization of nanophotonic Bragg-grating devices is important for their applications in large-scale integrated photonic systems,[8,9,45] since most CMOS-compatible active devices, such as high-speed optical modulators and detectors, are developed on submicron SOI wafers.[46] Tunable delay lines on submicron silicon were recently demonstrated using PS gratings[38] and serial/step-chirped gratings,[45] where the delay was tuned by changing laser wavelength. These devices work in reflection mode, which require optical circulators for system applications.

In order to achieve low-loss, on-chip tunable delay lines, we designed a linearly chirped contra-DC.[47] The schematic is shown in Fig. 12. Both the size and pitch of the perturbations on the slab are constant along the entire coupler. Linear chirping is achieved by tapering the waveguide widths. This uniform grating design ensures that lithographic effects are constant throughout the coupler, and thus can be more precisely predicted.[29] As the waveguides become narrower along the length of the coupler, the local phase-match condition (Eq. 1) shifts to shorter wavelengths. Therefore, various wavelengths travel different distances with distinct delays before being dropped to the output. For a fixed wavelength, we can change the effective indices, e.g., by the thermo-optic effect, and thus the position that satisfies the phase-match condition for the delay tuning.

As illustrated in Fig. 12(b), the ribs are linearly tapered from 620 nm (W_1) and 420 nm (W_2) to 600 nm (W_3) and 400 nm (W_4), respectively. Therefore, the two waveguides have a constant difference in width of 200 nm. Other parameters include a uniform pitch, Λ, of 310 nm, a coupler gap, G, of 600 nm, and a perturbation width, D, of 300 nm, which are all constant through the entire coupler for a uniform grating design. The entire coupler is 3.72 mm in length and 4 μm in width, giving a small footprint of 0.015 mm^2. The device was fabricated using e-beam lithography. The measured transmission spectrum is shown in Fig. 13(a). The group delay was measured by characterizing the waveforms generated by an external modulator with non-return-to-zero (NRZ) signals operating at 10 Gb/s, similar to the method used in.[40,45] The passband is 9.5-nm wide. The excess loss near the band edge at the short-wavelength side (1558 nm) is less than 2 dB, corresponding to the total loss though a round trip (7.44 mm) of the entire coupler, from which a propagation loss of 2.7 dB/cm is extracted. The range of the delay measurement was limited by the bandwidth of the EDFA used for compensating for the insertion losses of the FGCs and the modulator. A delay of 96 ps was measured at 1558 nm. Ripples are observed in both the transmission and delay spectra, which can be suppressed using grating apodization.

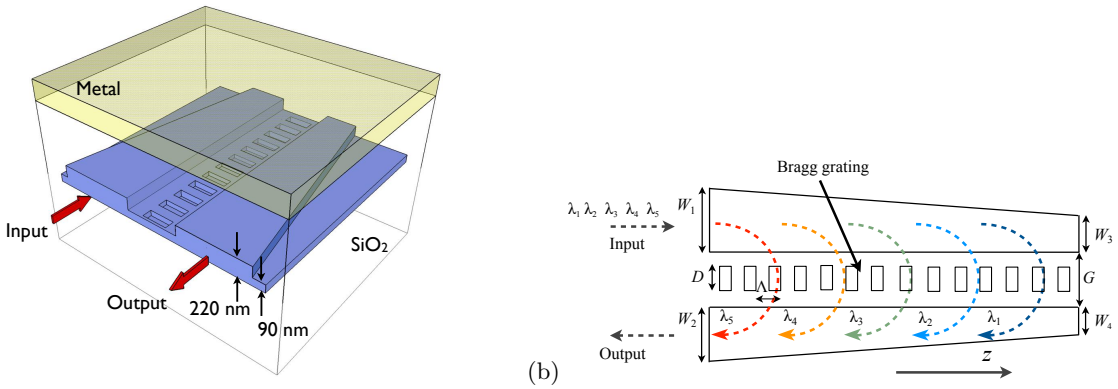

Figure 12. Schematic of the tunable optical delay line using contra-DCs in rib waveguides with uniform Bragg gratings: (a) perspective view; (b) top view.

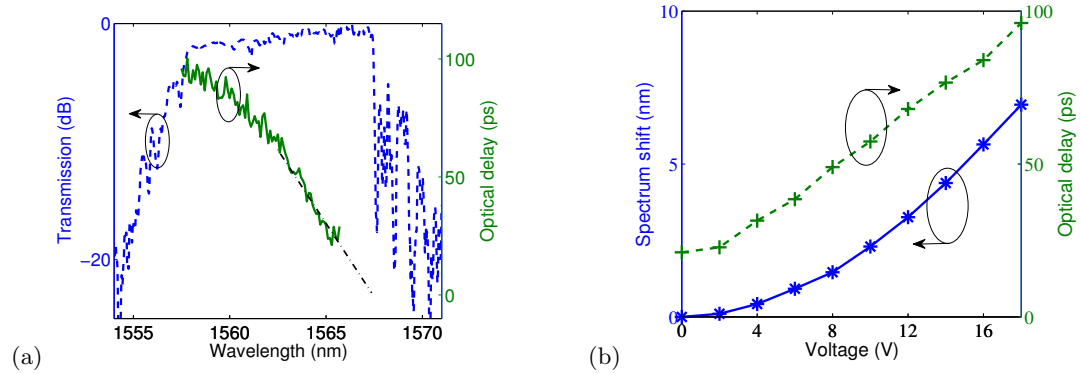

Figure 13. (a) Measured transmission and group delay of the proposed photonic delay line; (b) Tuning of the spectrum and group delay for $\lambda = 1565.3\ nm$.

The delay has a slope of −11 ps/nm, indicating a negative chromatic dispersion, D, of −3 ps/(nm·mm). While the maximal bit rate, B_{max}, depends on modulation formats and receiver design, the chromatic dispersion limit can be estimated for NRZ pulses by:[48]

$$B_{max}(\text{in Gb/s}) = \sqrt{\frac{10^5}{|D| \cdot L}} \tag{7}$$

where L is the dispersive waveguide length and is equal to 3.72 mm for the maximal delay, which results in a bit rate greater than 95 Gb/s for 96 ps of delay. Higher bit rates are feasible for lower delays.

Improved system performance is anticipated when this device is used together with other components that have positive dispersions (e.g., optical fibers). Specifically, this device is able to compensate for the dispersion induced by a 647-m-long standard single-mode optical fiber with a chromatic dispersion of 17 ps/(nm·km). The negative dispersion can also be used for on-chip pulse compression.[24] The loss per unit delay is 20 dB/ns, higher than that of micrometer-scale Bragg gratings[44] due to stronger sidewall scattering. Recent progress in SOI waveguides has shown very low losses of below 0.1 dB/cm,[49] which may lead to a significantly reduced loss per unit delay of below 1 dB/ns. Also, the device length can be reduced by using a spiral structure.[12]

For proof-of-concept, a metal layer is deposited on top of the cladding for thermal tuning. The measured results with a fixed wavelength of 1565.3 nm are shown in Fig. 13(b). As the voltage increases, the spectrum red shifts and, accordingly, the group delay increases. Continuous delay tuning from 21 to 96 ps has been obtained with the spectrum shifted by over 7 nm. A delay below 21 ps is also feasible, but was not measured due to the bandwidth of the EDFA. Using the thermal tuning coefficient 0.09 nm/K,[33] the local temperate on the chip is estimated to be increased by 78 K for the maximum delay, leading to a thermal tuning coefficient of 1 ps/K.

4. CONCLUSION

In summary, we have reviewed our recent work on silicon photonic contra-DCs and their applications in optical communications. We presented the systematic analysis and optimization of grating-assisted contra-DCs on the submicron SOI platform. Our work significantly improved the state of the art in integrated Bragg filters. Using a novel anti-reflection grating design, we experimentally obtained single-band (i.e., no limitation of FSR) add-drop operation across 200 nm, which enables unlimited scalability of WDM channels. It was shown that the coupler design also allows for flexible phase and magnitude engineering of Bragg filters by manipulating the curvatures of photonic waveguides, which may have higher tolerance to fabrication errors. Using this method, we demonstrated coupler-apodized Bragg grating filters and achieved a record sidelobe suppression ratio of 30 dB on the submicron SOI platform. We further demonstrated an ultra-compact (0.008 mm^2), four-channel CWDM (de-)multiplexer that shows flat-top responses (1 dB bandwidth: 8–10 nm), insertion loss of < 1 dB, and low crosstalk of -23 dB. These wide-band WDM filters are very tolerant to temperature fluctuations (up to $\pm\ 50^0$C), which may significantly reduce power consumption of silicon photonic WDM links.

In addition to WDM filters, contra-DCs can be used for many applications (e.g., photonic resonators) conventionally based on reflective operation of Bragg gratings. Replacing two-port Bragg gratings with contra-DCs allows for direct integration (i.e., without using circulators) with other photonic devices such as lasers and modulators, as well as combining these functions to realize on-chip optical signal processors and photonic microwave systems. In particular, we demonstrated an integrated tunable delay line using chirped contra-DCs. Continuous tuning of optical group delay of up to 96 ps has been obtained, with a low insertion loss of less than 2 dB and a negative chromatic dispersion of -11 ps/nm that allows for bit rates of up to almost 100 Gb/s at the maximal delay. The device has a small footprint of 0.015 mm^2, and can be used for on-chip optical buffering, dispersion compensation, and pulse compression. These results show that contra-DCs are promising for large-scale integration of various Bragg-grating defined functions on silicon. Future work includes using these nanophotonic components to increase the complexity of integrated photonic circuits and realize systems such as optical interconnect transceivers and microwave-photonics processors.

ACKNOWLEDGEMENTS

We acknowledge CMC Microsystems, for enabling the fabrication through ePIXfab, and Lumerical Solutions, Inc., for providing the simulation software (MODE Solutions). We thank Xu Wang, Han Yun, Charlie Lin, Jonas Flueckiger, and Yun Wang with the University of British Columbia, as well as David Patel and Qiuhang Zhong with McGill University for their help in layout design and measurement. We also thank Tom Baehr-Jones and Michael Hochberg with the University of Delaware for the access to the BAE Systems foundry and for the assistance in the measurement of the PS contra-DCs. The e-beam lithography and related fabrication were conducted by Richard Bojko at the University of Washington Microfabrication/Nanotechnology User Facility, a member of the NSF National Nanotechnology Infrastructure Network. We thank E. Huante-Ceron and A. Knights with McMaster University for the metallization of the tunable delay line. This work was supported by the Natural Sciences and Engineering Research Council of Canada, particularly the SiEPIC program.

REFERENCES

[1] Othonos, A. and Kalli, K., [*Fiber Bragg Gratings: Fundamentals and Applications in Telecommunications and Sensing*], Artech House (May 1999).

[2] Painchaud, Y., Paquet, C., and Guy, M., "Optical tunable dispersion compensators based on thermally tuned fiber Bragg gratings," *Optics and Photonics News* **18**(9), 48–53 (2007).

[3] Cliche, J.-F., Painchaud, Y., Latrasse, C., Picard, M.-J., Alexandre, I., and Têtu, M., "Ultra-narrow Bragg grating for active semiconductor laser linewidth reduction through electrical feedback," in [*Bragg Gratings, Photosensitivity, and Poling in Glass Waveguides*], *Bragg Gratings, Photosensitivity, and Poling in Glass Waveguides* , BTuE2, Optical Society of America (2007).

[4] Rochette, M., Guy, M., LaRochelle, S., Lauzon, J., and Trepanier, F., "Gain equalization of EDFA's with Bragg gratings," *Photonics Technology Letters, IEEE* **11**, 536–538 (May 1999).

[5] Wang, C. and Yao, J., "Fiber Bragg gratings for microwave photonics subsystems," *Opt. Express* **21**, 22868–22884 (Sep 2013).

[6] Giuntoni, I., Stolarek, D., Gajda, A., G. Winzer, J. B., Tillack, B., Petermann, K., and Zimmerman, L., "Integrated drop-filter for dispersion compensation based on SOI rib waveguides," March.

[7] Tan, D. T. H., Ikeda, K., and Fainman, Y., "Cladding-modulated Bragg gratings in silicon waveguides," *Opt. Lett.* **34**(9), 1357–1359 (2009).

[8] Wang, X., Shi, W., Yun, H., Grist, S., Jaeger, N. A. F., and Chrostowski, L., "Narrow-band waveguide Bragg gratings on SOI wafers with CMOS-compatible fabrication process," *Optics Express* **20**(14), 15547–15558 (2012).

[9] Simard, A. D., Belhadj, N., Painchaud, Y., and LaRochelle, S., "Apodized silicon-on-insulator Bragg gratings," *Photonics Technology Letters, IEEE* **24**(12), 1033–1035 (2012).

[10] Wang, X., Shi, W., Grist, S., Yun, H., Jaeger, N. A. F., and Chrostowski, L., "Narrow-band transmission filter using phase-shifted Bragg gratings in SOI waveguide," in [*Photonics Conference (PHO), 2011 IEEE*], 869–870 (October 2011).

[11] Painchaud, Y., Poulin, M., Latrasse, C., and Picard, M., "Bragg grating based Fabry-Perot filters for characterizing silicon-on-insulator waveguides," in [*Group IV Photonics (GFP), 2012 IEEE 9th International Conference on*], 180–182 (Aug 2012).

[12] Simard, A. D., Painchaud, Y., and LaRochelle, S., "Integrated Bragg gratings in spiral waveguides," *Opt. Express* **21**, 8953–8963 (Apr 2013).

[13] Wang, X., Shi, W., Vafaei, R., Jaeger, N. A. F., and Chrostowski, L., "Uniform and sampled Bragg gratings in SOI strip waveguides with sidewall corrugations," *IEEE Photon. Technol. Lett.* **23**, 290–292 (2011).

[14] Veerasubramanian, V., Beaudin, G., Giguere, A., Le Drogoff, B., Aimez, V., and Kirk, A., "Design and demonstration of apodized comb filters on SOI," *Photonics Journal, IEEE* **4**, 1133–1139 (Aug 2012).

[15] Yeh, P. and Taylor, H. F., "Contradirectional frequency-selective couplers for guided-wave optics," *Appl. Opt.* **19**, 2848–2855 (1980).

[16] Weber, J.-P., "Spectral characteristics of coupled-waveguide Bragg-reflection tunable optical filter," *Optoelectronics, IEE Proceedings J* **140**, 275–284 (October 1993).

[17] Hong, J. and Huang, W., "Coupled-waveguide exchange-Bragg resonator filters: Coupled-mode analysis with loss and gain," *Journal of Lightwave Technology* **11**(2), 226–233 (1993).

[18] Riziotis, C. and Zervas, M. N., "Design considerations in optical add/drop multiplexers based on grating-assisted null couplers," *Journal of Lightwave Technology* **19**(1), 92–104 (2001).

[19] Qiu, M., Mulot, M., Swillo, M., Anand, S., Jaskorzynska, B., and Karlsson, A., "Photonic crystal optical filter based on contra-directional waveguide coupling," *Applied Physics Letters* **83**, 5121–5124 (2003).

[20] Tan, D. T. H., Ikeda, K., and Fainman, Y., "Coupled chirped vertical gratings for on-chip group velocity dispersion engineering," *Appl. Phys. Lett.* **95**, 141109 (2009).

[21] Shi, W., Wang, X., Zhang, W., Chrostowski, L., and Jaeger, N. A. F., "Contradirectional couplers in silicon-on-insulator rib waveguides," *Optics Letters* **36**, 3999–4001 (2011).

[22] Tan, D. T. H., Ikeda, K., Zamek, S., Mizrahi, A., Nezhad, M. P., Krishnamoorthy, A. V., K. Raj, J. E. C., Zheng, X., Shubin, I., Luo, Y., and Fainman, Y., "Wide bandwidth, low loss 1 by 4 wavelength division multiplexer on silicon for optical interconnects," *Optics Express* **19**, 2401–2409 (2011).

[23] Shi, W., Wang, X., Yun, H., Zhang, W., Chrostowski, L., and Jaeger, N., "Add-drop filters in silicon grating-assisted asymmetric couplers," in [*Optical Fiber Communication Conference*], *Optical Fiber Communication Conference* , OTh3D.3, Optical Society of America (2012).

[24] Tan, D. T. H., Sun, P., and Fainman, Y., "Monolithic nonlinear pulse compressor on a silicon chip," *Nature Communications* **1**(16), 116 (2010).

[25] Shi, W., Wang, X., Zhang, W., Yun, H., Lin, C., Chrostowski, L., and Jaeger, N. A. F., "Grating-coupled silicon microring resonators," *Appl. Phys. Lett.* **100**, 121118 (2012).

[26] Shi, W., Greenberg, M., Wang, X., Lin, C., Jaeger, N. A. F., and Chrostowski, L., "Single-band add-drop filters using anti-reflection, contradirectional couplers," August.

[27] Shi, W., Wang, X., Lin, C., Yun, H., Liu, Y., Baehr-Jones, T., Hochberg, M., Jaeger, N. A. F., and Chrostowski, L., "Electrically tunable resonant filters in phase-shifted contra-directional couplers," *IEEE Group IV Photonics Conference (San Diego, CA, USA 2012), paper WP2* .

[28] Shi, W., Wang, X., Lin, C., Yun, H., Liu, Y., Baehr-Jones, T., Hochberg, M., Jaeger, N. A. F., and Chrostowski, L., "Silicon photonic grating-assisted, contra-directional couplers," *Optics Express* **21**(3), 3633–3650 (2013).

[29] Shi, W., Yun, H., Lin, C., Flueckiger, J., Jaeger, N. A. F., and Chrostowski, L., "Coupler-apodized Bragg-grating add–drop filter," *Opt. Lett.* **38**, 3068–3070 (Aug. 2013).

[30] Shi, W., Yun, H., Lin, C., Greenberg, M., Wang, X., Wang, Y., Fard, S. T., Flueckiger, J., Jaeger, N. A. F., and Chrostowski, L., "Ultra-compact, flat-top demultiplexer using anti-reflection contra-directional couplers for CWDM networks on silicon," *Opt. Express* , 6733–6738 (Mar 2013).

[31] Wang, X., Shi, W., Hochberg, M., Schelew, K. A. E., Young, J. F., Jaeger, N. A. F., and Chrostowski, L., "Lithography simulation for the fabrication of silicon photonic devices with deep-ultraviolet lithography," *IEEE Group IV Photonics Conference (San Diego, CA, USA 2012), paper ThP17* .

[32] Simard, A. D., Ayotte, N., Painchaud, Y., Bédard, S., and LaRochelle, S., "Impact of sidewall roughness on integrated Bragg gratings," *Journal of Lightwave Technology* **29**(24), 3693–3704 (2011).

[33] Shi, W., Vafaei, R., Á. G. Torres, M., Jaeger, N. A. F., and Chrostowski, L., "Design and characterization of microring reflectors with a waveguide crossing," *Optics Letters* **35**, 2901–2903 (2010).

[34] Feng, D., Qian, W., Liang, H., Kung, C.-C., Fong, J., Luff, B. J., and Asghari, M., "Fabrication insensitive echelle grating in silicon-on-insulator platform," *IEEE Photon. Technol. Lett.* **23**(5), 284– 286 (2011).

[35] Chen, L., Buhl, L., and Chen, Y., "Eight-channel SiO_2/Si_3N_4/Si/Ge CWDM receiver," *IEEE Photon. Technol. Lett.* **23**(17), 1201–1203 (2011).

[36] Brouckaert, J., Roelkens, G., Selvaraja, S. K., Bogaerts, W., Dumon, P., Verstuyft, S., Thourhout, D. V., and Baets, R., "Silicon-on-insulator CWDM power monitor/receiver with integrated thin-film InGaAs photodetectors," *IEEE Photon. Technol. Lett.* **21**(19), 1423–1425 (2009).

[37] Bock, P. J., Cheben, P., Schmid, J. H., Velasco, A. V., Delâge, A., Janz, S., Xu, D.-X., Lapointe, J., Hall, T. J., and Calvo, M. L., "Demonstration of a curved sidewall grating demultiplexer on silicon," *Optics Express* **20**(18), 19882–19892 (2012).

[38] Burla, M., Cortés, L. R., Li, M., Wang, X., Chrostowski, L., and Azaña, J., "Integrated waveguide Bragg gratings for microwave photonics signal processing," *Opt. Express* **21**, 25120–25147 (Oct 2013).

[39] Yao, J., "A tutorial on microwave photonics," *IEEE Photonics Society Newsletter* **26**(3), 5–12 (2012).

[40] Xia, F., Sekaric, L., and Vlasov, Y., "Ultracompact optical buffers on a silicon chip," *Nature Photonics* **1**, 65–71 (2006).

[41] Melloni, A., Canciamilla, A., Ferrari, C., Morichetti, F., O'Faolain, L., Krauss, T., De La Rue, R., Samarelli, A., and Sorel, M., "Tunable delay lines in silicon photonics: Coupled resonators and photonic crystals, a comparison," *Photonics Journal, IEEE* **2**(2), 181–194 (2010).

[42] Morton, P. A., Cardenas, J., Khurgin, J. B., and Lipson, M., "Fast thermal switching of wideband optical delay line with no long-term transient," *Photonics Technology Letters, IEEE* **24**(6), 512–514 (2012).

[43] Khan, S., Baghban, M. A., and Fathpour, S., "Electronically tunable silicon photonic delay lines," *Optics Express* **19**(12), 11780–11785 (2011).

[44] Giuntoni, I., Stolarek, D., Kroushkov, D. I., Bruns, J., Zimmermann, L., Tillack, B., and Petermann, K., "Continuously tunable delay line based on SOI tapered Bragg gratings," *Optics Express* **20**(10), 11241–11246 (2012).

[45] Spasojevic, M. and Chen, L. R., "Discretely tunable optical delay lines using serial and step-chirped sidewall Bragg gratings in SOI," *Electronics Letters* **49**, 608–610 (Apr 2013).

[46] Reed, G. T., Mashanovich, G., Gardes, F. Y., and Thomson, D. J., "Silicon optical modulators," *Nature Photonics* **4**, 518 – 526 (2010).

[47] Shi, W., Veerasubramanian, V., Patel, D., and Plant, D. V., "Tunable nanophotonic delay lines using linearly chirped contradirectional couplers with uniform bragg gratings," *Opt. Lett.* **39**, 701–703 (Feb 2014).

[48] Kaminow, I. and Li, T., [*Optical fiber telecommunications IV-B: systems and impairments*], Academic press (2002).

[49] Bogaerts, W. and Selvaraja, S., "Compact single-mode silicon hybrid rib/strip waveguide with adiabatic bends," *Photonics Journal, IEEE* **3**(3), 422–432 (2011).